



HAL
open science

Unsteady three-dimensional numerical simulations of methane combustion in dense fluidized bed

Ziad Hamidouche, Enrica Masi, Pascal Fede, Olivier Simonin, Renaud Ansart,
Mehrdji Hemati

► **To cite this version:**

Ziad Hamidouche, Enrica Masi, Pascal Fede, Olivier Simonin, Renaud Ansart, et al.. Unsteady three-dimensional numerical simulations of methane combustion in dense fluidized bed. 9th International Conference on Multiphase Flow (ICMF 2016), May 2016, Firenze, Italy. pp. 1-6. hal-01706943

HAL Id: hal-01706943

<https://hal.science/hal-01706943>

Submitted on 12 Feb 2018

HAL is a multi-disciplinary open access archive for the deposit and dissemination of scientific research documents, whether they are published or not. The documents may come from teaching and research institutions in France or abroad, or from public or private research centers.

L'archive ouverte pluridisciplinaire **HAL**, est destinée au dépôt et à la diffusion de documents scientifiques de niveau recherche, publiés ou non, émanant des établissements d'enseignement et de recherche français ou étrangers, des laboratoires publics ou privés.



Open Archive TOULOUSE Archive Ouverte (OATAO)

OATAO is an open access repository that collects the work of Toulouse researchers and makes it freely available over the web where possible.

This is an author-deposited version published in : <http://oatao.univ-toulouse.fr/>
Eprints ID : 19500

To link to this article : DOI:

URL :

To cite this version : Hamidouche, Ziad and Masi, Enrica and Fedé, Pascal and Simonin, Olivier and Ansart, Renaud and Hemati, Mehdi *Unsteady three-dimensional numerical simulations of methane combustion in dense fluidized bed*. (2016) In: 9th International Conference on Multiphase Flow (ICMF 2016), 22 May 2016 - 27 May 2016 (Firenze, Italy).

Any correspondence concerning this service should be sent to the repository administrator: staff-oatao@listes-diff.inp-toulouse.fr

Unsteady three-dimensional numerical simulations of methane combustion in dense fluidized bed

Ziad Hamidouche¹, Enrica Masi^{1*}, Pascal Fede¹, Olivier Simonin¹, Renaud Ansart² and Mehrdji Hemati²

¹Institut de Mécanique des Fluides de Toulouse (IMFT), Université de Toulouse, CNRS, INPT, UPS, Toulouse, France

²Laboratoire de Génie Chimique, Université de Toulouse, CNRS, INPT, UPS, Toulouse, France

Abstract

Natural gas combustion in dense fluidized beds containing inert particles involves complex physical mechanisms related to the bed hydrodynamic coupling with the gaseous combustion. In their experiments, Dounit et al. (Powder Technology, 2008) reported that for bed temperatures lower than a critical value (< 850 °C), almost all the combustion takes place above the bed surface. In the present study, detailed unsteady 3D CFD simulations of such experiments have been performed using NEPTUNE_CFD code, which is based on an Euler-Euler approach to compute both gas and solid phases. Time-averaged quantities were computed and compared with the available experimental measurements. The numerical results (gas temperature and gaseous-species molar fractions in and above the bed) are found to be very sensitive to the mesh refinement in such reactive dense gas-particle flows.

Keywords: Reactive multiphase flows, fluidized bed, natural gas combustion

1. Introduction

Fluidized-beds reactors are widely used in many industrial applications, especially in solid treatment applications where energy may be supplied by direct combustion of fossil fuels inside the bed itself. Thanks to its low sulphur content, natural gas is the least polluting fossil fuel. In addition, working at relatively low temperature allows to minimize combustion pollutants, especially NO and NO_2 emissions. Given this ecological benefit, it appears of great interest to understand and master natural gas combustion process in fluidized beds. The present study is a theoretical/numerical investigation of air-methane combustion in a dense fluidized-bed reactor for which experimental results are available by the works of Dounit et al. [3, 4, 5]. The experimental setup consisted of a reactor of 180 mm in diameter and 1400 mm in height, above which, a disengagement section of 360 mm in diameter is added. The experiments were conducted using sand particles with mean diameter $350\mu\text{m}$ and density 2650 kg/m^3 . In order to maintain a constant temperature in the bed, cooling air may circulate in a double shell. A detailed description of the experiments may be found in the aforementioned publications.

2. Modeling approach

An Euler-Euler approach is used to describe both the gaseous and the particulate phases by solving a set of mean equations for each phase (mass, momentum and enthalpy equations). Coupling between the phases is accounted for through interphase transfer terms (see Ref. [14, 15] for more details). In addition, species transport equations and a state law are used to predict the gaseous species evolution and the change in gas density.

2.1. Mass, momentum and enthalpy balance equations

For each phase, the balance equations are written as follows :

$$\frac{\partial}{\partial t}(\alpha_k \rho_k) + \frac{\partial}{\partial x_j}(\alpha_k \rho_k U_{k,j}) = 0 \quad (1)$$

$$\alpha_k \rho_k \left(\frac{\partial U_{k,i}}{\partial t} + U_{k,j} \frac{\partial U_{k,i}}{\partial x_j} \right) = -\alpha_k \frac{\partial P_g}{\partial x_i} + \alpha_k \rho_k g_i + I_{k' \rightarrow k,i} - \frac{\partial \Sigma_{k,ij}}{\partial x_j} \quad (2)$$

$$\alpha_k \rho_k \left(\frac{\partial H_k}{\partial t} + U_{k,j} \frac{\partial H_k}{\partial x_j} \right) = \frac{\partial}{\partial x_j} \left(\alpha_k \rho_k K_k \frac{\partial H_k}{\partial x_j} \right) + \Pi_{k' \rightarrow k} + S_{rad,k} \quad (3)$$

In Eqn (1), α_k represents the volume fraction of the phase k (which may be either the gas and in that case $k = g$, or the particulate phase in which case $k = p$). ρ_k and $U_{k,j}$ are the phase's density and velocity respectively.

In Eqn (2), P_g is the local mean gas pressure and g_i is the gravity. $I_{k' \rightarrow k,i}$ accounts for the interfacial momentum transfer between the phases and the last term is the transport due to the velocity fluctuations. Details concerning the closures of these last two terms may be found in Ref. [2, 8].

In Eqn (3), H_k represents the total enthalpy of the phase k . The first term on the right hand side (r.h.s.) is an enthalpy transport term written in the frame of the gradient approximation with an effective thermal diffusivity, K_k [10, 11]. The convection/diffusion heat transfer term ($\Pi_{k' \rightarrow k}$ in the r.h.s. of Eqn (3)) is modeled according to :

$$-\Pi_{p \rightarrow g} = \Pi_{g \rightarrow p} = -\frac{\alpha_p \rho_p C_{pp}}{\tau_{gp}^T} (T_p - T_g) \quad (4)$$

where T_g and T_p are the local mean gaseous and particulate phase temperatures, respectively. τ_{gp}^T is the thermal characteristic time scale defined as :

$$\frac{1}{\tau_{gp}^T} = \frac{6\lambda_g}{\rho_p C_{pp}} \frac{\langle Nu \rangle_p}{d_p^2} \quad (5)$$

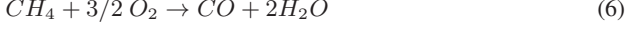
in which λ_g is the gas thermal conductivity. The Nusselt number of the particulate phase is defined as $\langle Nu \rangle_p = 2 + 0.55 Re_p^{1/2} Pr^{1/3}$ where $Pr = \rho_g \nu_g C_{pg} / \lambda_g$ is the Prandtl number and $Re_p = \alpha_g \langle |\mathbf{v}_r| \rangle_p d_p / \nu_g$ is the mean particle Reynolds

*corresponding author: emasi@imft.fr

number (\mathbf{v}_r refers to the relative velocity vector). Finally, the last term in Eqn (3), $S_{rad,k}$, represents the heat exchange due to thermal radiation in the reactor. Its model is given in section (2.4).

2.2. Combustion modeling

Methane combustion is described by the following global two-step mechanism :



which is modeled by the following two-step kinetic mechanism proposed by Dryer and Glassman [6] :

$$R_1 = 10^{10.2} \exp\left(-\frac{48400}{R_g T_g}\right) [CH_4]^{0.7} [O_2]^{0.8} \quad (8)$$

$$R_2 = 10^{10.25} \exp\left(-\frac{43000}{R_g T_g}\right) [CO][H_2O]^{0.5} [O_2]^{0.25} \quad (9)$$

In Eqn (8 and 9), the kinetic rates (R_1 and R_2) have units of mol/m³/s and the species molar concentrations are given in mol/m³. R_g is the ideal gas constant (8.314 J mol⁻¹ K⁻¹).

2.3. Balance of species of the gaseous mixture

In the numerical simulations, the gaseous mixture is composed of $N = 6$ species which are : methane, oxygen, nitrogen, carbon dioxide, carbon monoxide and water vapor.

The gaseous mixture mass conservation and the local composition evolution were predicted using only 5 (rather than 6) transport equations. In addition, knowing that the atomic species are always conserved during any chemical process, it was then decided to transport the atomic mass fractions of the atomic species C , H and N . They are related to the mass fractions of the mixture gas species by the following relations : $Y_C = 12/16 Y_{CH_4} + 12/28 Y_{CO} + 12/44 Y_{CO_2}$, $Y_H = 4/16 Y_{CH_4} + 2/18 Y_{H_2O}$ and $Y_N = Y_{N_2}$. The remaining two species computed by the numerical simulations are CH_4 and CO . The transport equation of each species is written as follows :

$$\alpha_g \rho_g \left(\frac{\partial Y_\alpha}{\partial t} + U_{g,j} \frac{\partial Y_\alpha}{\partial x_j} \right) = \frac{\partial}{\partial x_j} \left(\alpha_g \rho_g D_g \frac{\partial Y_\alpha}{\partial x_j} \right) + \Psi_\alpha \quad (10)$$

In the above equation, Y_α represents the mass fraction of the transported species while D_g is the turbulent diffusion coefficient. The last r.h.s. term accounts for the change in species mass fraction due to the reactions. Such a source term is equal to zero for the atomic species mass fractions ($\Psi_C = \Psi_H = \Psi_N = 0$). The vanishing rate of methane (in kg/m³/s) due to the reaction (6), is modeled according with Eqn (8) :

$$\Psi_{CH_4} = -\alpha_g W_{CH_4} R_1 \quad (11)$$

and the rate of change of carbon monoxide mass fraction has to account for both appearance and vanishing of such a species due to the reactions (6) and (7). It is modeled according with Eqn (9):

$$\Psi_{CO} = \alpha_g W_{CO} (R_1 - R_2) \quad (12)$$

The carbon dioxide and water vapor mass fractions (Y_{CO_2} and Y_{H_2O}) are deduced from the transported species while the oxygen mass fraction is computed according to the following conservation law :

$$Y_{O_2} = 1 - (Y_{CH_4} + Y_{H_2O} + Y_{CO_2} + Y_{CO} + Y_{N_2}) \quad (13)$$

With the assumption of a mixture of ideal gases within the reactor, the density of the gaseous mixture is governed by :

$$\rho_g = \frac{P_{ref}}{R_g T_g} \sum_{\alpha=1}^N \frac{Y_\alpha}{W_\alpha} \quad (14)$$

where W_α is the molar mass of the gaseous species α and P_{ref} is the reference pressure which is set to 101325 Pa.

2.4. Thermal radiation model

A simplified thermal radiation model was used in this study. It assumes that the gas does not absorb radiation and each radiating point has an unobstructed isotropic view of the surrounding cold [1]. Then, the radiation heat loss rate per unit volume may be written as follows :

$$S_{rad,g} = 4\sigma \sum_{\alpha=1}^n P_\alpha \beta_\alpha \epsilon_{bulk} (T_{bulk}^4 - T_g^4) \quad (15)$$

where σ is the Stefan-Boltzmann constant (5.669×10^{-8} W m⁻² K⁻⁴). P_α and β_α are the partial pressure in atmosphere unit and the Planck mean absorption coefficient of the species α , respectively. T_{bulk} and ϵ_{bulk} are the surrounding medium temperature and emissivity, respectively. T_{bulk} is either the local mean particle temperature T_p or the reactor wall temperature T_W , according to a critical value of the solid volume fraction. In this study, we set:

$$(T_{bulk}, \epsilon_{bulk}) = \begin{cases} (T_p, \epsilon_p) & \text{if } \alpha_p \geq 0.02 \\ (T_W, \epsilon_W) & \text{otherwise} \end{cases} \quad (16)$$

ϵ_p and ϵ_W are the particles and the wall emissivities, respectively. Four species ($n = 4$ in Eqn (15)) are retained in the calculation and they are water vapor, carbon dioxide, carbon monoxide and methane. Their absorption coefficients are made varying as a function of the gas temperature according to the curve fits proposed in the literature [1, 9, 16]. Regarding the solid phase, the heat loss due to the particles' radiation toward the reactor walls is taken into account only in the dilute regions ($\alpha_p < 0.02$) and it is computed as follows :

$$S_{rad,p} = 4\sigma \beta_p \epsilon_W (T_W^4 - T_p^4) \quad (17)$$

where the particle absorption coefficient is $\beta_p = 3\epsilon_p \alpha_p / (2d_p)$.

3. Numerical simulation

Unsteady three dimensional numerical simulations of the fluidized-bed reactor are performed using the Eulerian N-fluid modeling approach for fluid-particle turbulent polydispersed reactive flows implemented in NEPTUNE_CFD V1.08@Tlse version by IMFT (Institut de Mécanique des Fluides de Toulouse). NEPTUNE_CFD is a computational multiphase flow software developed in the framework of the NEPTUNE project, financially supported by CEA (Commissariat à l'Énergie Atomique), EDF (Electricité de France), IRSN (Institut de Radioprotection et de Sécurité Nucléaire) and AREVA-NP. The performances of NEPTUNE_CFD for high parallel computing are highlighted in Ref. [12].

3.1. Configuration and mesh

A sketch of the retained configuration is shown by Fig. 1(a). It consists of a cylindrical reactor of diameter 180 mm and height 1400 mm completed with an above disengaging section of diameter 360 mm and height 520 mm. Concerning the reactor mesh, four grid refinements were tested. They are referred to as MESH0, MESH1, MESH2 and MESH3 and their characteristics are summarized in Table 1. For the last three meshes, Δz is set to the value indicated in Table 1 for a coordinate $z \leq 80$ cm while it is chosen as 2.5 cm for $z \geq 90$ cm and a gradual connection

inside the range $80 < z < 90$ cm is realized. As an example, MESH1 is depicted in Fig. 1(b).

Table 1: Mesh characteristics

	Units in cm			Number of cells
	Δx	Δy	Δz	
MESH0	0.820	1.560	2.500	31185
MESH1	0.820	1.560	1.250	45979
MESH2	0.820	1.560	0.625	72114
MESH3	0.400	0.740	0.300	583071

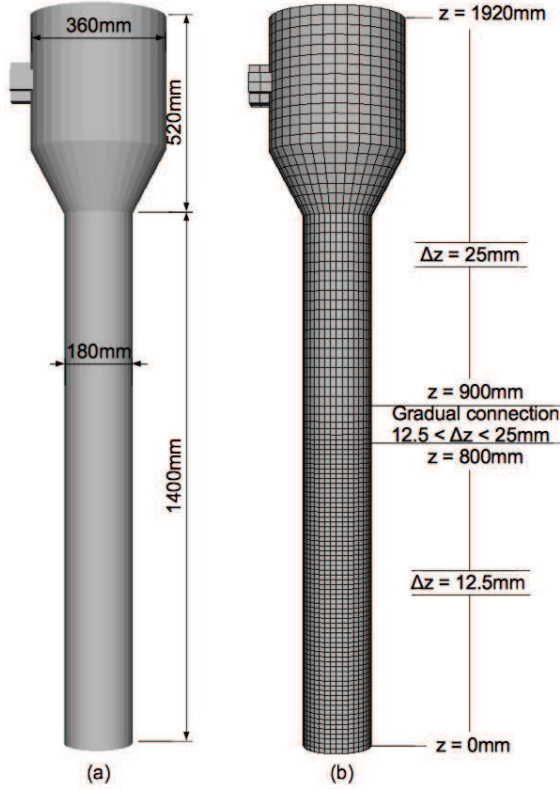


Figure 1: (a) Reactor geometry, (b) Reactor MESH1.

3.2. Numerical parameters

The quantities of interest for the numerical simulations are summarized in Tables 2 and 3. Only one class of sand particles was retained with a diameter representing the mean diameter of the sample used in the experiments (ranging between 315 and 400 μm [4]). In the experiments, a distributor composed of a perforated plate of 0.4% porosity is used. Its effect in the numerical simulations is reproduced by assuming a perfect air-methane mixing at the reactor inlet. Such an assumption is justified by the fact that the pressure drop induced by the distributor is comparable to that induced by the particle bed (which suggests a uniform gas distribution at the reactor inlet).

Table 2: Thermodynamic gaseous species properties

Species	C_p ($\text{J mol}^{-1} \text{K}^{-1}$)	ΔH_f^0 (kJ mol^{-1})
CH_4	35.796	-74.8
H_2O	35.744	-241.82
CO_2	39.089	-393.52
CO	29.195	-110.58
O_2	29.426	0
N_2	29.173	0

At the initialization, a solid mass of 12 kg and a bed temperature of 700 $^\circ\text{C}$ were imposed. Found to be very effective boundary conditions in dense fluidized beds for spherical particles bouncing on a very rough wall [7], no-slip condition for the mean particle velocity combined with zero-flux condition for the particle kinetic energy were selected in our simulations. For all the numerical simulations, the same kinetic mechanism of Dryer and Glassman [6] (as presented in section 2.2) is used. Numerical simulations will thus refer to as DG_700_MESH0,1,2 and 3.

3.3. Results and discussions

All simulations have been made run for 80 seconds in order to ensure to reach a permanent regime. In such a regime, particles and the fluid properties are supposed to be statistically stationary and mean (time-averaged) quantities may be computed for an analysis purpose. Figure 2 shows the mean pressure drop along the reactor height as predicted from the numerical simulations, compared to the experimental data. Globally, the pressure-drop is very well reproduced. Some differences in value are instead observed (and estimated to be around 5 %) at the bottom bed. These differences may be attributed to the elutriation phenomenon and to the uncertainty in experimental measurements.

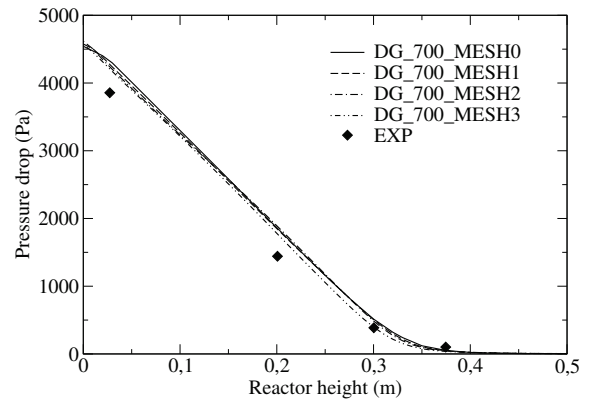


Figure 2: Numerical against experimental mean pressure drop

For all the simulations, mean gas temperature profiles are depicted in Fig. 3(a) (at the center, $X = 0$ m) and Fig. 3(b) (at the wall, $X = 0.09$ m). Experimental measurements are also displayed for comparison. Pre et al. [13] and Dounit et al. [3, 4, 5] pointed out that for bed temperatures lower than 850 $^\circ\text{C}$, the combustion zone moves towards the freeboard region and over. At the operating point of 700 $^\circ\text{C}$, one expects that most of the combustion takes place at the freeboard. This is indeed what observed when looking at the results illustrated by Fig. 3. However, some differences are found when comparing numerical results with experimental measurements. The first difference concerns the maximum of the gas temperature as predicted at the freeboard. A substantial deviation from the experiments is observed when the coarsest grid is used (MESH0). For this mesh, the gas temperature exhibits strong radial inhomogeneities. In particular, temperature predictions near the wall are strongly overestimated. Such a poor resolution has in fact an important effect on the modeling of the solid near the wall. The correct prediction of the local solid amount is in fact crucial in order to accurately reproduce the combustion process. Improved results are obtained when using finer grids. For instance, the gas temperature radial inhomogeneities are drastically reduced when MESH2 is employed, which leads to obtain very close maxima of the temperature at the freeboard. Comparing the maxima of gas temperature as predicted by the coarsest and the finest grids (DG_700_MESH0 and DG_700_MESH3) a difference of about 115 $^\circ\text{C}$ and 340 $^\circ\text{C}$ is

Table 3: Gas and particle properties

Gas properties		Particle properties	
Mixture composition	Air and methane	Density, ρ_p	2650 kg m ⁻³
Total flow rate	14.6 Nm ³ h ⁻¹	Mean diameter, d_p	350 μ m
Air factor, Φ	1.2	Restitution coefficient, e_c	0.9
Fluidizing velocity, U_f	$2U_{mf}$ at 298 K	Radiative emissivity, ϵ	0.6
Minimum fluidization velocity, U_{mf}	0.08 m s ⁻¹ at 298 K		

found at the center and near the wall, respectively. This difference is noteworthy. Despite the ability of all the meshes to reproduce the good bed expansion for this class of particles, accurate heat transfers may only be obtained by a finer grid refinement. This is due to the necessity to reproduce the local particulate behavior as better as possible in order to ensure accurate local heat exchanges and thus correct combustion ignition.

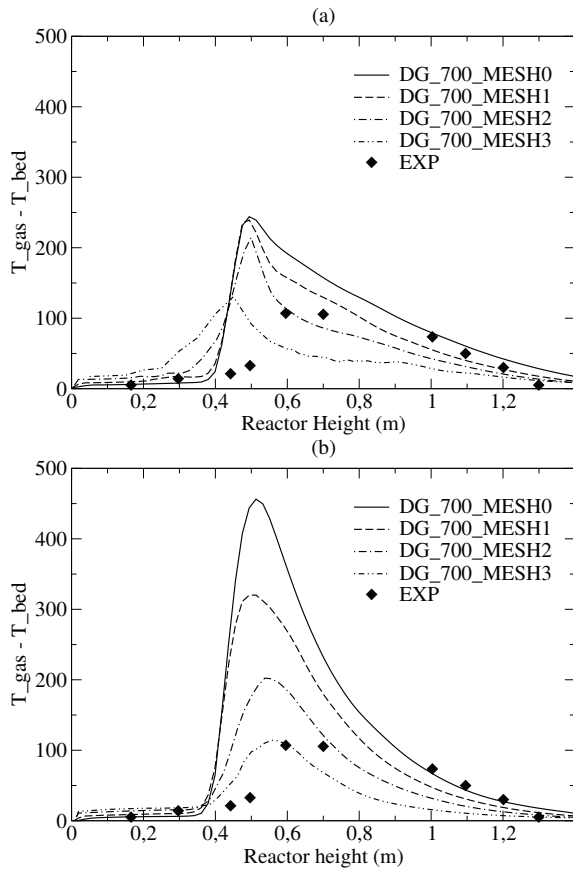


Figure 3: Numerical against experimental mean gas temperature

A second difference between the numerical results and the experimental measurements concerns the position of the combustion zone. Globally, for the finest grids, such a position is quite well predicted near the wall. However, a moving towards the bed is observed at the reactor center. In the experiments, cooling air is circulating in a double shell which encloses the reactor over a height of about 80 cm in order to maintain a constant temperature in the bed. In our simulations, heat exchanges with the wall in the bed were not accounted for. It is well known that finer refinements make it possible to predict the bubbling behavior into the bed and the eruption behavior at the freeboard with a high fidelity. This leads to better reproduce the gas pockets in the bed and their explosion at the bed surface. It is also well known that in the gas pockets the combustion process is enhanced and that the

solid acts instead like a quenching for the combustion. As an evidence of such a mechanism, snapshots of the instantaneous gas temperature and solid volume fraction are depicted in Fig. 4 for MESH3. In the figure, inverted transfer functions are used for the color map, thus light zones correspond to high gas temperature (on the left) and low solid volume fraction (on the right).

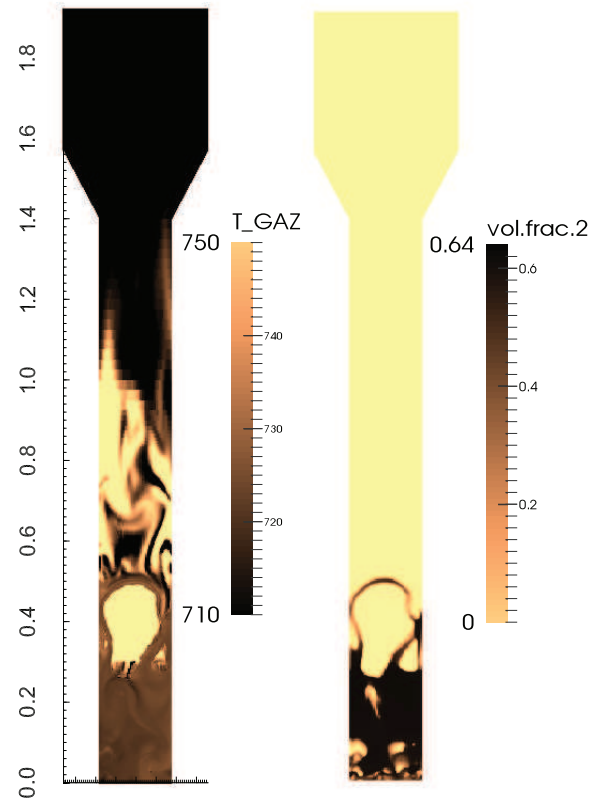


Figure 4: Snapshots of the instantaneous gas temperature ($^{\circ}$ C) and the instantaneous particle volume fraction, at time = 65.2 s.

Instantaneous fields show that, into the bed, the temperature is higher in the gas pockets meaning that combustion is favoured in such zones, leading to a faster conversion rate. For the same instant ($t=65.2$ s), a scatter plot of the instantaneous gas temperature ($T_g - T_{bed}$) versus the solid volume fraction is computed for MESH3 into the bed ($z \leq 40$ cm) and results depicted in Fig. 5. Results show that the lower is the particle volume fraction (corresponding to the bubble zones) the higher is the temperature into the bed. Consistent results are found concerning the fuel conversion. In the experiments, gas samples are taken at the center of the reactor using sampling tubes connected to the cooling unit in order to eliminate the steam. Species molar fractions are then measured by means of infrared or paramagnetic type analyzers depending on the species. In Fig. 6, profiles of the mean methane molar fractions at the reactor center are shown.

As expected, methane conversion is overestimated into the bed for MESH3 while it is quite well reproduced for the other grid refinements (even the coarsest one). Above the bed, results show that the methane molar fraction is underestimated by all the simulations since methane have already reacted. For the coarser grids, this is consistent with the observations about the gas temperature overestimate at the freeboard; in this region, methane conversion is faster compared to the experimental measurements.

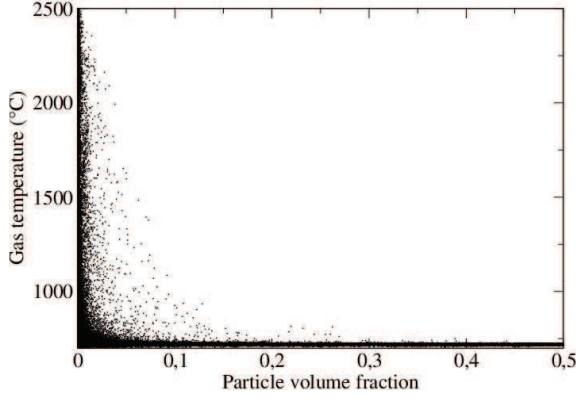


Figure 5: Scatter plot of the instantaneous gas temperature ($T_g - T_{bed}$) as a function of the particle volume fraction into the bed ($z \leq 40$ cm).

The effect of the mesh size on thermodynamics and reactions may also be observed by Fig. 7 in which iso-contours of the local and instantaneous gas temperature are superposed to local and instantaneous solid volume-fraction fields for two different mesh sizes (MESH0 and MESH3). Once again, higher temperatures are found into the bed when the finest mesh is used because of the better resolution of the bed hydrodynamics. It is clear that the latter has a strong effect on the temperature predictions inside the bed and at the freeboard as well.

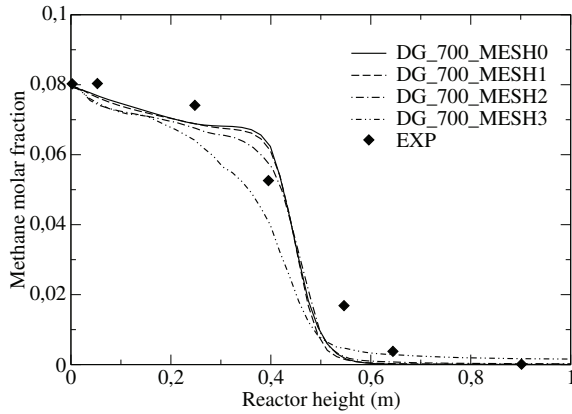


Figure 6: Numerical against experimental methane mean molar fraction

In order to quantify the effect of the bed hydrodynamics (i.e., the local particle volume fraction resolution) on the temperature predictions, a total enthalpy budget analysis of the gas-solid mixture is carried out in the region including the freeboard (spanning from 30 cm to 55 cm). For both the gas and the particle phases, Eqn (3) is written in a conservative form and the total enthalpy equation (particles+gas) is computed and integrated over such a

region when the permanent regime is reached. After simplifications, a final equation using mean quantities is written as follows:

$$\Delta \bar{T}_g = -\frac{\Delta \bar{H}_f^0}{C_{pg}} - \frac{\overline{\alpha_p \rho_p U_p^+}}{\alpha_g \rho_g U_g} \frac{C_{pp} \Delta \bar{T}_p}{C_{pg}} - \frac{(\bar{S}_{rad,p} + \bar{S}_{rad,g})V}{\alpha_g \rho_g U_g C_{pg} A} \quad (18)$$

where \bar{T}_g and \bar{T}_p are mean (spatial and temporal averaged) gas and particle temperatures, C_{pg} is the mean gas specific heat capacity, V and A are the region volume and the normal to axial direction area, and $\bar{S}_{rad,p}$ and $\bar{S}_{rad,g}$ the mean amount of all the radiative terms. Equation (18) shows that the mean gas temperature increment is mainly due to three contributions which are the heat release from combustion, a contribution due to the bed hydrodynamics and a radiative source term. This equation may be written in the synthetic form as:

$$\Delta \bar{T}_g = \Delta \bar{T}_{g,COMB} - \Delta \bar{T}_{g,HYDR} - \Delta \bar{T}_{g,RAD} \quad (19)$$

The above three contributions were estimated in all the simulations. Results obtained from MESH0 and MESH2 are here given, as an example:

MESH0:

$$\Delta \bar{T}_{g,COMB}=1864 \text{ K}; \quad \Delta \bar{T}_{g,HYDR}=604 \text{ K}; \quad \Delta \bar{T}_{g,RAD}=183 \text{ K}$$

MESH2:

$$\Delta \bar{T}_{g,COMB}=1762 \text{ K}; \quad \Delta \bar{T}_{g,HYDR}=791 \text{ K}; \quad \Delta \bar{T}_{g,RAD}=234 \text{ K}$$

As expected, the combustion contribution for MESH0 is larger than that computed from MESH2. This is consistent with the observations about the gas temperature overestimate at the freeboard for MESH0. But most important, results show that the hydrodynamic contribution plays an important role in the gas temperature predictions, more than the radiative contribution, and that an accurate prediction of the bed hydrodynamic is mandatory for accurately predict reactive fluidized beds.

4. Conclusion

In this study, an Euler-Euler approach was used to perform unsteady 3D numerical simulations of methane combustion in a fluidized-bed reactor containing inert particles. Four meshes were tested in order to investigate the influence of the mesh refinement on the combustion. Comparisons between numerical and experimental data pointed out a strong dependency of the gas temperature predictions on the mesh refinement. This dependency is attributable to the hydrodynamic resolution of the bed. Finer mesh make it possible to reproduce the bubble-eruption behavior of the mixture, strongly affecting the heat exchange into the bed and at the bed surface. Numerical results also showed that when a refined mesh is used, because of the better resolution of the gas pockets into the bed which implies an increase of the gas temperature at such locations, heat exchanges between the bed and the wall have to be accounted for by an appropriate model in order to maintain the operational bed temperature. This point is crucial and deserves to be further investigated.

5. Acknowledgements

This work received funding from the European Community through the SUCCESS project under the 7th Framework program (Grant agreement No. 608571). It reflects only the author's views and the Community is not liable for any use that may be made of the information contained therein. This work was granted access to the HPC resources of CALMIP supercomputing center under the allocation 2015 – 0111. CALMIP is gratefully acknowledged.

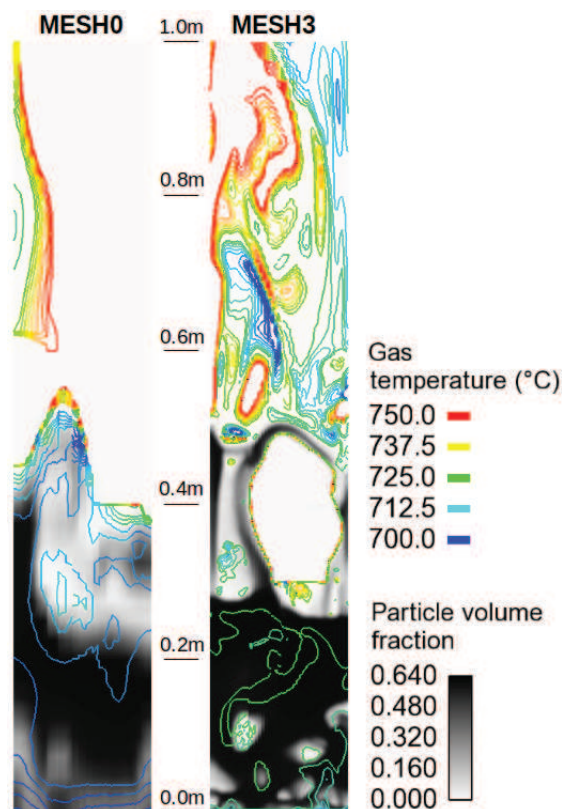


Figure 7: Snapshots of the instantaneous gas temperature ($^{\circ}\text{C}$) and the instantaneous particle volume fraction, at time = 65.2 s.

References

- [1] Barlow, R.S., Karpetsis, A.N., Frank, J.H. and Chen, J.-Y., Scalar profiles and no formation in laminar opposed-flow partially premixed methane/air flames, *Combustion and Flame*, 127, pp. 2102-2118, 2001.
- [2] Boëlle, A., Balzer, G. and Simonin, O., Second-order prediction of the particle-phase stress tensor of inelastic spheres in simple shear dense suspensions, *In Gas-Particle Flows*, ASME FED, 228, pp. 9-18, 1995.
- [3] Dounit, S., Hemati, M. and Steinmetz, D., Natural gas combustion in fluidised bed reactors between 600 and 850 $^{\circ}\text{C}$: experimental study and modelling of the freeboard, *Powder Tech.*, 120, pp. 49-54, 2001a.
- [4] Dounit, S., *Combustion of natural gas in fluidised bed reactor: experimental study and modelling of dense and disengagement zones*, Phd Thesis, INPT, 2001b.
- [5] Dounit, S., Hemati, M. and Andreux, R., Modelling and experimental validation of a fluidized-bed reactor freeboard region : Application to natural gas combustion, *Chem. Eng. J.*, 140, pp. 457-465, 2008.
- [6] Dryer, F.L., and Glassman, I., High temperature oxidation of CO and CH_4 , *14th Symp. Int. Combustion*, 14, pp. 987-1003, 1973.
- [7] Fede, P., Simonin, O. and Ingram, A., 3D numerical simulation of a lab-scale pressurized dense fluidized bed focussing on the effect of the particle-particle restitution coefficient and particle - wall boundary conditions, *Chem. Eng. Sci.*, 142, pp 215-235, 2016.
- [8] Gobin, A., Neau, N., Simonin, O., Llinas, J.R., Reiling, V. and Selo, J.L., Fluid dynamic numerical simulation of a gas phase polymerization reactor, *Inter. Journal for Numerical Methods in Fluids*, 43, pp. 1199-1220, 2003.
- [9] Grosshandler, W. L., *RADCAL: A Narrow-Band Model for Radiation Calculations in a Combustion Environment*, NIST technical note 1402, 1993.
- [10] Konan, A., Neau, H., Simonin, O., Dupoizat, M. and Le Goaziou, T., Reactive Multiphase Flow Simulation of Uranium Hexafluoride Conversion Reactor, *7th International Conference on Multiphase Flow*, Tampa, FL, May 30 - June 4, 2010a.
- [11] Konan, N.A., Neau, H., Simonin, O., Dupoizat, M. and Le Goaziou, T., 3D Unsteady Multiphase Simulation of Uranium Tetrafluoride Particle Fluorination in Fluidized Bed Pilot, *Proceedings of the 20th International Conference on Fluidized Bed Combustion*, Guangxi Yue, Hai Zhang, Changsui Zhao, Zhongyang Luo (Eds.), Springer Berlin Heidelberg, pp. 1152-1158, 2010b.
- [12] Neau, H., Fede, P., Laviéville, J. and Simonin, O., High Performance Computing (HPC) for the Fluidization of Particle-Laden Reactive Flows, *14th International Conference on Fluidization-From Fundamentals to Products*, Eds, ECI Symposium Series, 2013.
- [13] Pre, P., Hemati, M. and Marchand, B., Study on natural gas combustion in fluidized beds : modelling and experimental validation, *Chem. Eng. Sci.*, 53, pp. 2871-2883, 1998. 53, 2871-2883, 1998.
- [14] Simonin, O., Deutsch, E. and Minier, J.P., Eulerian prediction of the fluid/particle correlated motion in turbulent two-phase flows, *Applied Scientific Research*, 51, pp. 275-283, 1993.
- [15] Simonin, O., *Statistical and continuum modelling of turbulent reactive particulate flows*, Von Karman Institute for Fluid Dynamics, Rhode Saint Genèse, Belgium, 2000.
- [16] Web site of the International Workshop on Measurement and Computation of Turbulent Nonpremixed Flames (TNF), <http://www.sandia.gov/TNF/radiation.html>